13

Interactive Optimisation of a Flywheel

The first aim of this chapter is to present how multi-objective optimisation (MOO) (see Chap. 3) and global approximation (GA) (see Chap. 4) can be employed in order to speed up and improve the design of complex mechanical system. The second aim of this chapter is to propose a multi-objective interactive design methodology (see Sect. 3.6) based on Pareto surface sensitivity analysis. This methodology has been implemented by a software where the designer interacts with the multi-objective programming software to choose the preferred final solution especially suited for applications where computer simulations can reliably predict the properties of a system.

Many real-world engineering design problems involve the simultaneous optimisation of several conflicting objectives. Design engineers are often interested in identifying the Pareto-optimal set [166] when exploring a design space.

By considering Definition (2.7) of non-dominated solution the outcome of a MOO is not one optimal point but a set of Pareto-optimal solutions that represent the trade-off between objectives. A solution in a Pareto-optimal set cannot be considered better with respect to others in the set without including preference information to rank competing attributes. Interactive optimisation tasks (see Sect. 3.6) can help the designer (i.e. the decision maker) to define this ranking function.

This chapter develops a Pareto-optimisation method for use in real-world optimisation problems. This method is based on coupling design performances, expressed by objective functions and obtained by simulating the process to optimise, with approximation concepts [88,104,159,202] (see Chap. 4). Often the numerical analysis to obtain the objective function considered is computationally expensive, especially for large complex systems. Approximation concepts may help to limit the required analyses during the optimisation. The basic idea is to build approximation of the response-based objective functions and constraints that can be easily evaluated by the optimiser, without resorting to numerical analysis.

The approximating model may be an interface that may also open new ways to make the design optimisation of engineering system more controllable and accessible compared with a direct coupling of optimisation and analysis.

Another important remark that should be stressed is that the method presented gives a strong importance to the sampling of design variables to generate good approximation models. The techniques presented are based on Quasi-Monte Carlo sampling methods [183,246] (see Sect. 3.4.2). The sampling plain of design variables is a somewhat well-distributed plain to maximise the amount of information that can be obtained from a single numerical analysis.

This chapter shows how the Pareto-optimal set can be locally analysed through Pareto sensitivity analysis to eventually restrict the field of search of the final solution by the decision maker. This information is used by an interactive method [166] that allows the designer to compare the first solution with an alternative solution obtained by moving locally around the first solution. The final solution results from an interaction between the designer and the optimisation software. During this process the designer learns the possible performances of his system and can formulate in a satisfactory manner the target of his project.

This chapter will be dedicated to explain the interactive optimisation method and an illustrative example, based on the optimisation of a flywheel, will be shown.

13.1 System Model

The example illustrates the use of the proposed interactive optimisation strategies (Sect. 3.6). It deals with the design of a flywheel for enhanced dynamic, cost and structural performance.

The general aim of the optimal design of this mechanical component is to reduce, at a given rotational speed, the mass, the maximum stress and to increase the energy stored by the flywheel. This problem has been studied extensively in design literature [18, 84, 121, 131]. In this example the flywheel profile is defined by a spline curve. Complete structural analyses of the flywheel should be comprehensive both for the analysis of the shaft and the analysis of the flywheel. For reasons of simplicity the analyses are confined to wheel. The computation of the stresses of the structure is performed by considering the axis-symmetric properties of the structure. The variable flywheel thickness $h(r)$ is considered small, so the stresses σ_z, τ_{zr} and $\tau_{z\theta}$ can be considered as null (see Fig. 13.1).

The forces acting on an infinitesimal volume of the structure are (see Fig. 13.1) as follows:

$$F_r = \sigma_r h r d\theta \tag{13.1}$$

$$F_\theta = \sigma_\theta (h + dh/2) dr \tag{13.2}$$

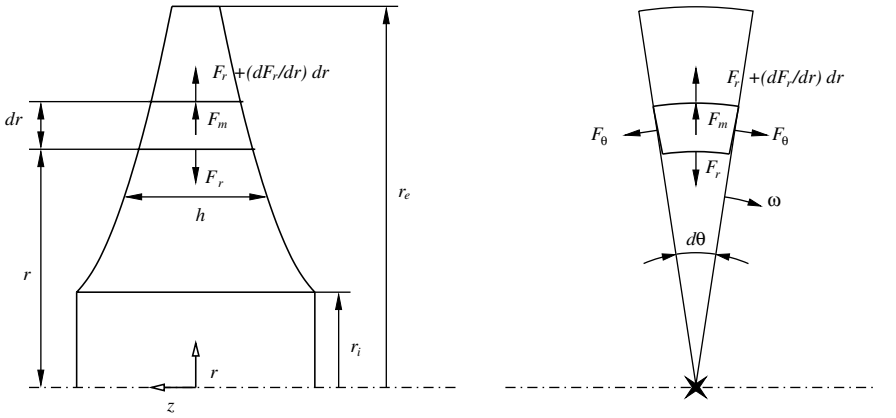

Fig. 13.1. Forces acting on a infinitesimal element of a flywheel having variable thickness

$$F_m = \rho\omega^2 r(h + dh/2)dr(r + dr/2)d\theta \tag{13.3}$$

The equilibrium along the radial direction gives

$$-F_r + F_r + \frac{dF_r}{dr}dr - 2F_\theta \sin\frac{d\theta}{2} + F_m = 0 \tag{13.4}$$

by substituting Eqs. (13.1)–(13.3) and neglecting the second-order terms

$$\frac{d}{dr}(\sigma_r hr) - \sigma_\theta h + \rho\omega^2 r^2 h = 0 \tag{13.5}$$

that are identically satisfied by introducing a stress function [249]:

$$\begin{aligned} \sigma_r &= \frac{\Gamma}{hr} \\ \sigma_\theta &= \frac{1}{h}\frac{d\Gamma}{dr} + \rho\omega^2 r^2 \end{aligned} \tag{13.6}$$

By considering the relations between strain and displacements we have

$$\begin{aligned} \varepsilon_r &= \frac{du}{dr} \\ \varepsilon_\theta &= \frac{u}{r} \end{aligned}$$

that, by eliminating u, becomes

$$\varepsilon_r - \frac{d}{dr}(\varepsilon_\theta r) = 0 \tag{13.7}$$

Consider the relationship between stress and strain

$$\varepsilon_r = \frac{1}{E}\sigma_r - \frac{\nu}{E}\sigma_\theta$$
$$\varepsilon_\theta = \frac{1}{E}\sigma_\theta - \frac{\nu}{E}\sigma_r$$

E is the Young's modulus and ν the Poisson's ratio. We can write Eq. (13.7) as a function of σ_r and σ_θ.

$$\sigma_r - \nu\sigma_\theta - \frac{d}{dr}(r(\sigma_\theta - \nu\sigma_r)) = 0 \tag{13.8}$$

We can perform the structural analysis by considering Eq. (13.8) only in the stress function

$$r^2\frac{d^2\Gamma}{dr^2} + r\frac{d\Gamma}{dr} - \Gamma + (3+\nu)\rho\omega^2 hr^3 = \frac{r}{h}\frac{dh}{dr}\left(r\frac{d\Gamma}{dr} - \nu\Gamma\right) \tag{13.9}$$

This equation cannot be solved analytically. This differential equation has been solved by using a fourth-order Runge–Kutta method and imposing the contour conditions at inner and outer radius ($\Gamma(r_i) = 0$, $\Gamma(r_e) = 0$). All integration points (h, dh/dr) necessary for the integration of Eq. (13.9) are obtained by considering h as a spline function of the radius. The failure criterion refers to Von Mises reference stress and is calculated by

$$\sigma_{VM} = \sqrt{((\sigma_r - \sigma_\theta)^2 + \sigma_r^2 + \sigma_\theta^2)/2} \tag{13.10}$$

If the stresses in the disk exceed the admissible value, failure occurs. The mass M is given by

$$M = 2\pi\rho\int_{r_i}^{r_e} hrdr \tag{13.11}$$

The kinetic energy K stored by the flywheel is obtained by the equation

$$K = \pi\rho\omega^2\int_{r_i}^{r_e} hr^3dr \tag{13.12}$$

13.2 Objective Functions

Optimising the flywheel design requires to maximise the kinetic energy and to minimise weight and stress level (near the admissible value). The multi-objective optimisation problem described is realised by transforming the objective function related to the maximum $\sigma_{VM} = \sigma_{VMM}$, the minimum mass M and the maximum kinetic energy K into a vector to be optimised.

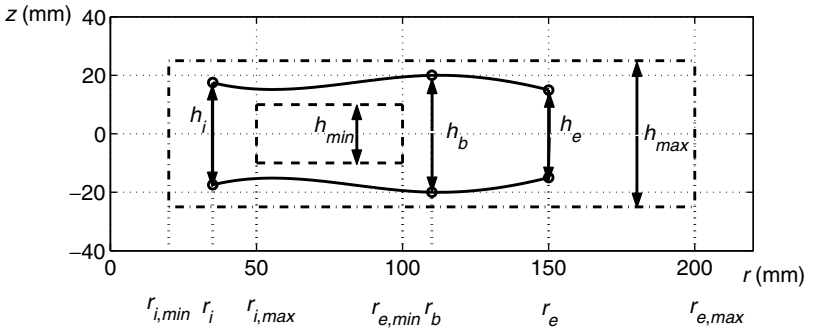

Fig. 13.2. Cross-section of the flywheel. Definition of design variables and design bounds

13.3 Design Variables

The design variables are defined as the coordinates of the control points of a cubic spline (see Fig. 13.2). These control points define the thickness of the flywheel over the entire area of the disk.

So we have the design variables vector (see Fig. 13.2)

$$\begin{aligned}\mathbf{x}^T &= (x_1, \ldots, x_8) \\ &= (r_i, r_e, r_b, h_i, h_e, h_b, (dh/dr)_i, (dh/dr)_e)\end{aligned}$$

by defining the smallest and the largest disk thickness respectively by h_m and h_M we can formulate the multi-objective optimisation problem as

$$\begin{aligned}&\min_{\mathbf{x}} \begin{bmatrix} f_1 \\ f_2 \\ f_3 \end{bmatrix} = \min_{\mathbf{x}} \begin{bmatrix} M \\ -K \\ \sigma_{VMM} \end{bmatrix} \\ &g_1 = -h_m + h_{min} \leq 0 \\ &g_2 = h_M - h_{max} \leq 0 \\ &g_3 = -r_b + r_i - \Delta r \leq 0 \\ &g_4 = r_b - r_e - \Delta r \leq 0 \\ &g_5 = \sigma_{VMM} - \sigma_{adm} \leq 0 \end{aligned} \tag{13.13}$$

with design variables bounds:

$$\begin{aligned}&0.02\,\mathrm{m} \leq r_i \leq 0.05\,\mathrm{m} \\ &0.1\,\mathrm{m} \leq r_e \leq 0.2\,\mathrm{m} \\ &0.02\,\mathrm{m} \leq r_b \leq 0.2\,\mathrm{m} \\ &0.02\,\mathrm{m} \leq h_i \leq 0.05\,\mathrm{m} \\ &0.02\,\mathrm{m} \leq h_e \leq 0.05\,\mathrm{m}\end{aligned}$$

$$0.02\,\mathrm{m} \leq h_b \leq 0.05\,\mathrm{m}$$
$$-1 \leq \left(\frac{dh}{dr}\right)_i \leq 0$$
$$-1 \leq \left(\frac{dh}{dr}\right)_e \leq 0$$

Problem (13.13) refers to a flywheel that must be constrained to stay in a bounded volume and with maximum stress level equal to σ_{adm}(Table 13.1) The objective function f_2 has been defined equal to $-K$ because the kinetic energy has to be maximised.

Table 13.1. Flywheel problem data

h_{min} (m)	0.02
h_{max} (m)	0.05
Δr (m)	0.025
σ_{adm} (MPa)	280
ν	0.3
ω (rad/s)	1,570
ρ (kg/m^3)	7,800

13.4 Results

The global approximation model was based on a radial basis function neural network (RBFNN) (see Sect. 4.6.2). By using 2,048 points a Quasi-Monte Carlo sequence has been integrated into the interactive Optimisation loop (see Fig. 3.22).

The accuracy of the global approximation model is shown in Figs. 13.3–13.5, where the comparison of the profile of a flywheel computed by using the global approximation model is compared with that of the original physical model.

As much as 10^6 extrapolated points were obtained from the global approximation model to derive a set of non-dominated points close to the Pareto-optimal set. This set has been used in the first step of the design process, to choose a preferential starting solution for the interactive optimisation process through a utility function. In this example, the utility function is defined (see Sect. 3.5.1) by using as target values

- $\tilde{f}_1$ the value of the mass of the flywheel ($\int_V \rho\, dV$) with the minimum mass. ($\mathbf{x} = (50\,\mathrm{mm}, 100\,\mathrm{mm}, 75\,\mathrm{mm}, 20\,\mathrm{mm}, 20\,\mathrm{mm}, 20\,\mathrm{mm}, 0, 0)$). $f_1^0 = 3.678$ kg.
- $\tilde{f}_2$ the value of the maximum kinetic energy of the flywheel with maximum kinetic energy ($\frac{1}{2}\int_V \rho r^2 \omega^2\, dV$)not considering boundaries on stresses. $\mathbf{x} = (20\,\mathrm{mm}, 200\,\mathrm{mm}, 110\,\mathrm{mm}, 50\,\mathrm{mm}, 50\,\mathrm{mm}, 50\,\mathrm{mm}, 0, 0)$.

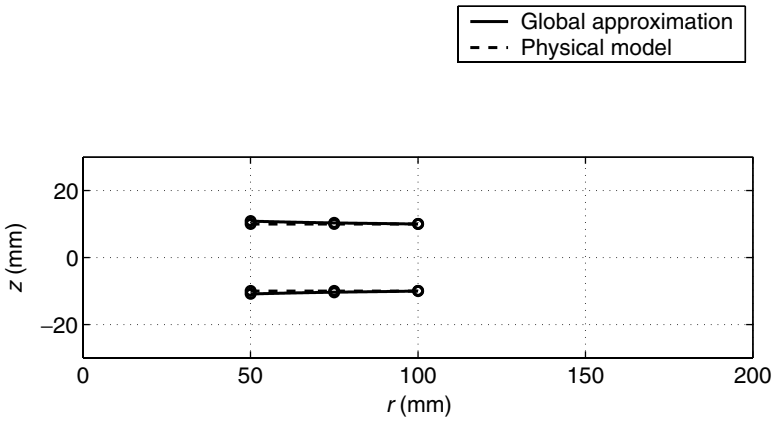

Fig. 13.3. Cross-section of the flywheel with the minimum mass obtained by optimising the global approximation model ('-') and the physical model ('- -')

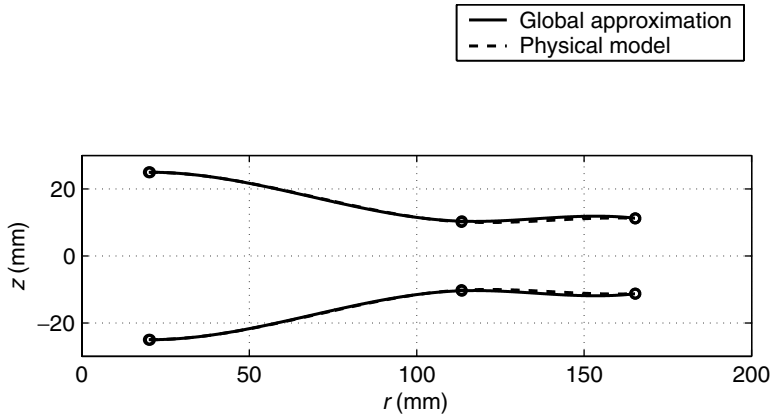

Fig. 13.4. Cross-section of the flywheel with the maximum kinetic energy obtained by optimising the global approximation model ('-') and the physical model ('- -')

$f_2^0 = 120.9 \times 10^{10}$ J.

- f_3 the limit stress of the flywheel considering as flywheel material C40 steel (UNI 7845 maximum admissible stress 420 MPa) and a safety margin of 1.5. So $f_3^0 = 280\,\text{MPa}$.

An optimal flywheel shape has been found by using the global approximation model (Fig. 13.6, the stresses are also plotted).

After that an optimal solution was found, this optimal solution will be taken into account as the reference optimal solution ('R'). The interactive optimisation procedure has been used where the designer explores the Pareto set in the neighbourhood of the current optimal solution. The interactive optimisation framework has been implemented in Matlab [153]. The solutions

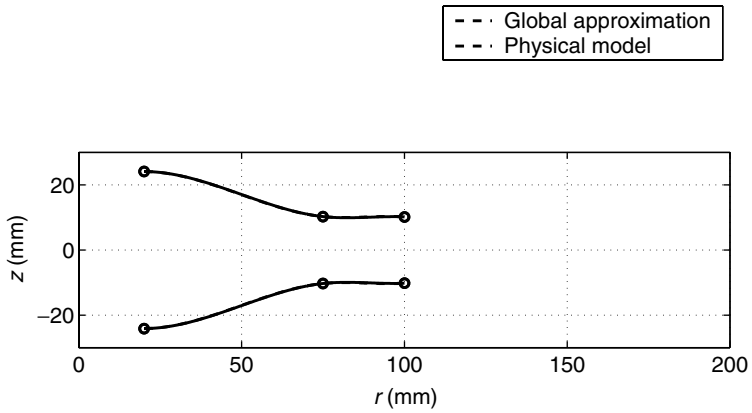

Fig. 13.5. Cross-section of the flywheel with the minimum level of stress (minimum σ_{rM}) obtained by optimising the global approximation model ('-') and the physical model ('- -')

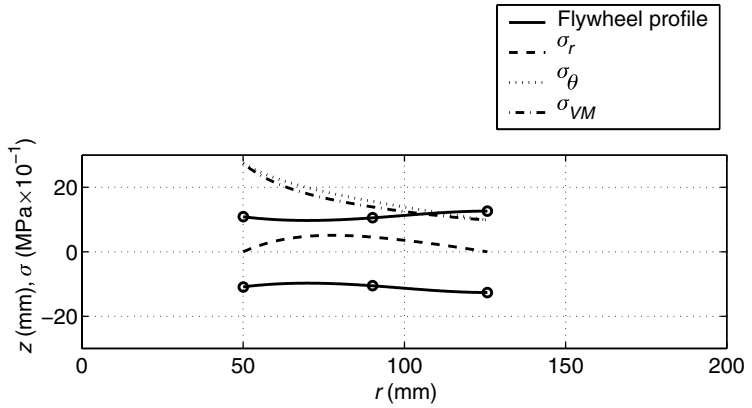

Fig. 13.6. Cross-section and stresses of the flywheel that optimise the utility function (see Sect. 3.5.1) by using the global approximation model. This optimal solution is taken as the reference optimal solution ('R' solution)

shown in Table 13.2 are those obtained by finding Pareto-optimal directions that minimise mass, maximise the stored kinetic energy and minimise the maximum stress.

Table 13.2 shows the results of the Pareto-optimal local sensitivity analysis of the solution shown in Fig. 13.6. The designer can look at this value to have an idea on how the direction in the predictor step (see Fig. 3.22) can influence the original solution.

Table 13.2. Pareto-optimal solutions obtained through utility function sensitivity analysis (remember that $\Delta f_2 > 0$ means a kinetic energy decrease)

	Δf_1 (kg)	Δf_2(J $\times 10^{10}$)	Δf_3 (MPa)
Solution 1	–0.161	0.280	–4.844
Solution 2	0.044	–0.076	0.935
Solution 3	–0.111	0.194	–7.319

The Δf_1, Δf_2, Δf_3 (see 13.13) are variations with respect to the reference optimal solution in Fig. 13.6

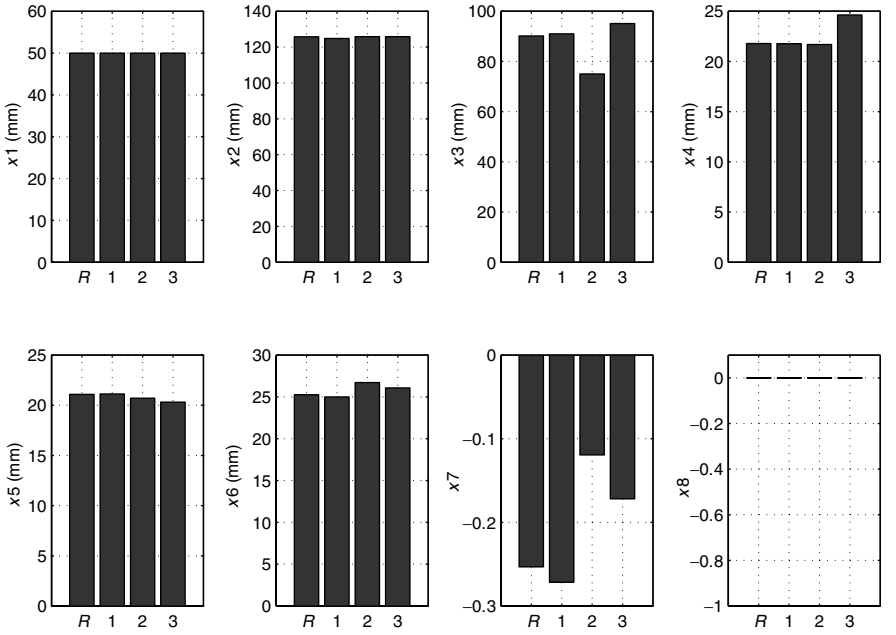

Fig. 13.7. Design variables of the reference solution (R) found during the interactive Pareto-optimal sensitivity analysis (Fig. 13.6). Solutions 1–3 refer to the corresponding solutions 1–3, in Table 13.2

The reference optimal solution (together with the solutions 1–3 in Table 13.2) is finally presented with bar charts (Figs. 13.7 and 13.8). This way of presenting the Pareto-optimal solutions clearly offers a better understanding on the trade-offs.

Following the procedure introduced in Sect. 3.6, the designer can find solutions 1–3 in Table 13.2 in a quick way, i.e. avoiding to complete the computation of the Pareto-optimal solutions by means of the physical system model but exploiting the global approximation model. In Figs. 13.9–13.11 a comparison is presented between Pareto-optimal solutions obtained by using

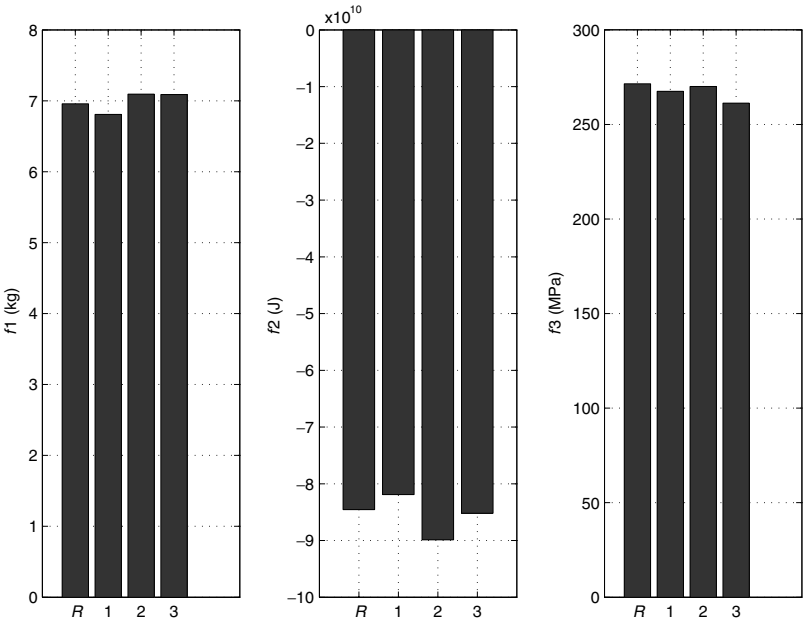

Fig. 13.8. Objective functions of the reference solution (R found during the interactive Pareto-optimal sensitivity analysis (Fig. 13.6). Solutions 1–3 refer to the corresponding solutions 1–3, in Table 13.2

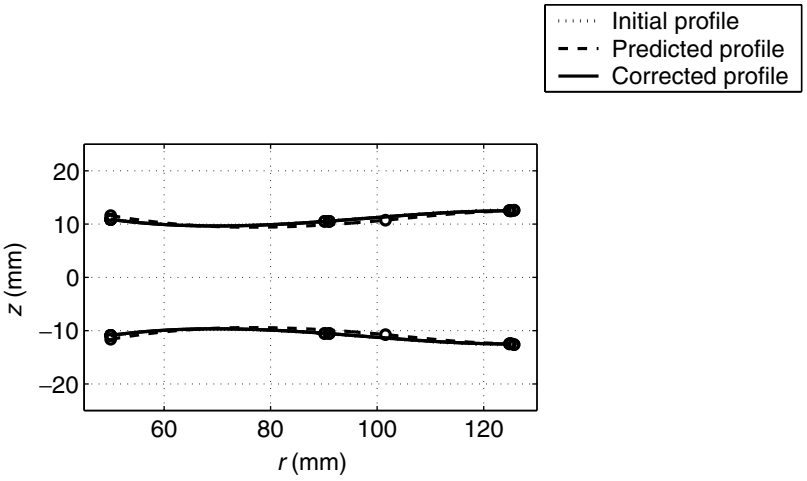

Fig. 13.9. Cross-section of the flywheel of Fig. 13.6 that optimises the utility function (see Sect. 3.5.1) by using the global approximation model compared to the solution obtained by using the prediction solution expressed by Eq. (3.58) choosing the direction that minimises more the flywheel mass and to the corrected solution obtained by solving the problem (3.59)

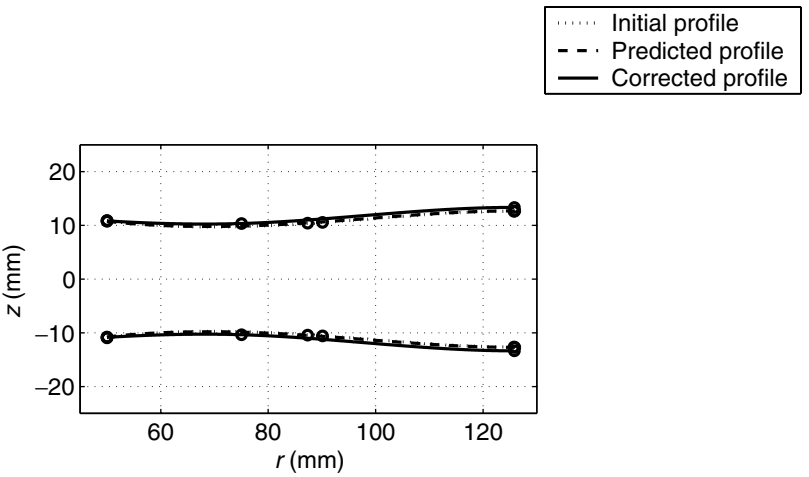

Fig. 13.10. Cross-section of the flywheel of Fig. 13.6 that optimises the utility function (see Sect. 3.5.1) by using the global approximation model compared to the solution obtained by using the prediction solution expressed by Eq. (3.58) choosing the direction that maximises more the flywheel kinetic energy and to the corrected solution obtained by solving the problem (3.59)

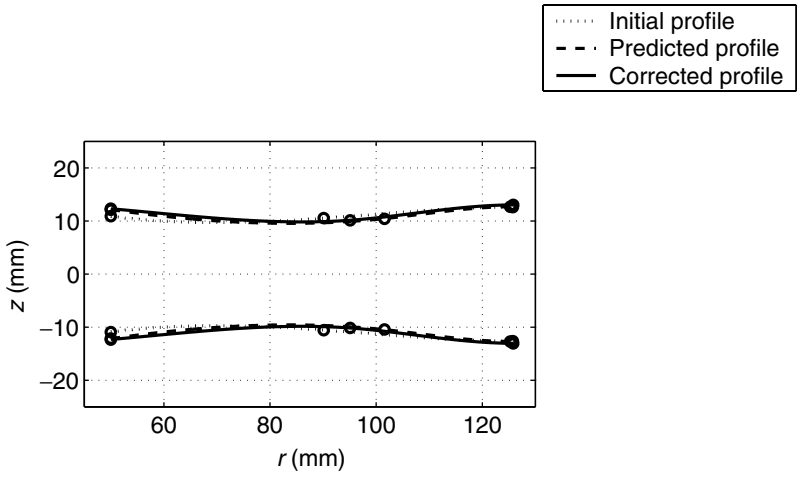

Fig. 13.11. Cross-section of the flywheel of Fig. 13.6 that optimises the utility function (see Sect. 3.5.1) by using the global approximation model compared to the solution obtained by using the prediction solution expressed by Eq. (3.58) choosing the direction that minimises more the flywheel maximum stress and to the corrected solution obtained by solving the problem (3.59)

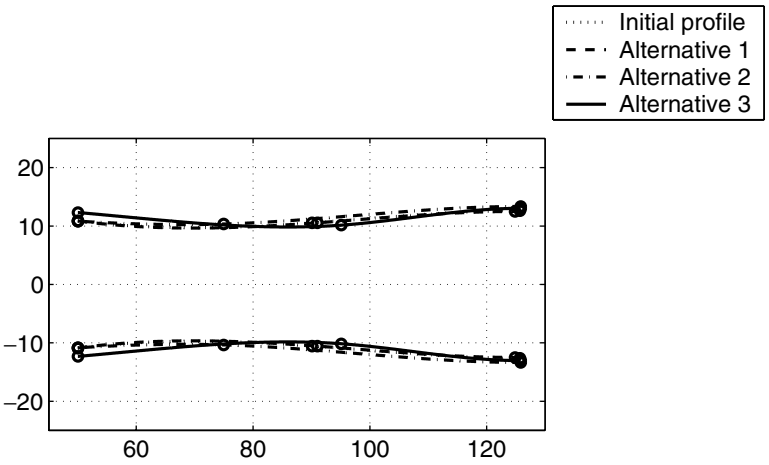

Fig. 13.12. Cross-section of the flywheel of Fig. 13.6 that optimise the utility function (see Sect. 3.5.1) by using the global approximation model compared to the alternative solution of Figs. 13.7 and 13.8.

the prediction framework presented in Sect. 3.6 (and shown in Figs. 13.7 and 13.8, also see Fig. 13.12) and Pareto-optimal solutions obtained by the global approximation model.

The designer can choose one of the solutions and eventually continue the Pareto sensitivity process proposed until a satisfying solution has been obtained.